J Mater Sci (2015) 50:374–381
DOI 10.1007/s10853-014-8596-2

Microstructures resulting from the interaction between ferrite recrystallization and austenite formation in dual-phase steels

D. Barbier · L. Germain · A. Hazotte · M. Gouné · A. Chbihi

Received: 27 June 2014 / Accepted: 8 September 2014 / Published online: 19 September 2014

Abstract The present work investigates the interactions between ferrite recrystallization and austenite formation in dual-phase steels by experiments performed at high heating rate (100 °C/s). It was shown that both ferrite recrystallization and austenite formation are strongly coupled and interdependent. The kinetics of ferrite recrystallization is strongly affected by the formation of austenite and can be even inhibited in some cases. The microstructure is more heterogeneous and anisotropic when both the austenite formation and the ferrite recrystallization overlap. It was highlighted that the degree of anisotropy depends on the volume fraction of austenite at a given temperature. Furthermore, an unusual behavior for austenite growth was highlighted. It is characterized by a much higher volume fraction than those obtained under OrthoEquilibrium and ParaEquilibrium. The results, especially those at 715 °C close to the eutectoid plateau, at which the driving force for austenite growth is classically low, suggest a diffusionless transformation for austenite.

D. Barbier · A. Chbihi
Arcelormittal Maizières Research SA, Voie Romaine, BP 30302, 57283 Maizières Les Metz, France

L. Germain · A. Hazotte · A. Chbihi
Laboratoire d'Étude des Microstructures et de Mécanique des Matériaux (LEM3), UMR CNRS 7239, Université de Lorraine - Île du Saulcy, 57045 Metz Cedex 1, France

L. Germain (✉) · A. Hazotte
DAMAS, Key Laboratory for Design of Alloy Metals for low-mAss Structures, Université de Lorraine, Nancy, France
e-mail: lionel.germain@univ-lorraine.fr

M. Gouné
ICMCB Bordeaux – UPR CNRS 9048I, 87 Avenue du Docteur Schweitzer, 33608 Pessac, France

Introduction

There is a continuous development of high-strength steels for automotive industry, under the conflicting objectives of lightening cars while ensuring low prices and high level of safety. This can be achieved by limiting the element addition while optimizing the microstructures. The currently mostly used low-alloyed high-strength steels are the so-called dual-phase (DP) steels [1–4]. DP steels are Fe–C–Mn alloys with a microstructure constituted by ferrite (α) and martensite (α') phases, which gives a good compromise between strength and ductility. This microstructure is directly obtained through continuous annealing at galvanizing line after the last cold-rolling step. More precisely, it is achieved by heating and soaking cold-rolled sheets in the ferrite/austenite (γ) domain—also called intercritical region—then cooling them rapidly to transform austenite to martensite. In an effort of designing the microstructure of DP steels, the formation of austenite in the intercritical region focused much attention [5–9]. Indeed, process parameters such as heating rate, soaking temperature, and holding time strongly influence the microstructure (volume fraction and topology of phases, grain size, etc.) which determines the final mechanical properties.

During heating rolled metal up to the soaking temperature, the austenite formation is preceded by ferrite recrystallization [10–13] and cementite (Fe_3C carbides) spheroidization [14]. Therefore, the austenite nucleates on dissolving globular cementite then grows at the expense of "fresh" ferrite [15–20]. In classical DP steels, austenite growth was shown to be controlled in a first step by carbon diffusion in austenite, then by manganese diffusion in ferrite, finally by partitioning of Mn in austenite [5]. Until recently, most studies devoted to austenite formation were concerned with "weak interaction" between ferrite

recrystallization and austenite formation. In that case, both phenomena do not overlap, and only the recrystallized ferrite grain size influences the austenite growth. However, as a consequence of recent evolutions of DP steel grades and process conditions, the ferrite recrystallization is progressively delayed toward or even above the temperature at which the austenite formation starts (Ac1). One way of inducing such "strong interaction" between recrystallization and austenite formation is to use rapid heating rates to reduce the processing time [21, 22]. Another one is to add microalloying elements such as Nb or B, which not only strengthens the steel by precipitation but also delays ferrite recrystallization [23, 24]. In any cases, this "strong interaction" results in significant changes in the final microstructures [25–31]. However, at the present time, the mechanisms driving this interaction need to be clarified, and the expected consequences on the resulting properties still lead to some controversies. This lack of knowledge mostly results from the difficulty to decorrelate the effects of a higher heating rate (increase of the nucleation density and of the driving force for transformation) from the competition between recrystallization and phase transformation. In a recent article [30], we tackled this question by applying different heating rates on a given DP steel (Fe-0.15wt%C-1.5 %Mn), inducing weak and strong interactions. We characterized and analyzed in detail the microstructure evolutions, and the involved mechanisms were discussed from both experimental and theoretical approaches. However, for sake of simplicity, this previous work only investigated one soaking temperature (740 °C). The present article relates the results of experiments in which only one heating rate was used (100 °C/s), leading to strong interaction, but different soaking durations and temperatures were tested, which results in significant changes in the final microstructure. In general, the whole results reported in the following are in agreement with our previous work [30] but some complementary valuable data and analysis are given concerning both the mechanisms of microstructure formation and the unusual behavior of austenite growth.

Material and experimental procedures

Material

The chemical composition of the laboratory casted steel is given in Table 1. This composition is typical of advanced high-strength steels with dual-phase microstructure (ferrite + martensite). The initial hot-rolled sheet exhibited a ferrite + pearlite microstructure. It was firstly rolled at room temperature to 75 % reduction. Then, heat treatments were applied to induce the interaction between ferrite recrystallization and austenite formation. They were performed on a DT 1000 Thermal Simulator from Adamel-Lhomargy, using samples with a section of 4 × 0.7 mm^2 and a length of about 12 mm. The temperature was controlled by a type-K thermocouple spot welded on the surface at the center of the sample. Continuous heating from room temperature was applied under argon gas at a rate of 100 °C/s. Four different soaking temperatures were studied: 680, 715, 740, and 780 °C. Samples were quenched from different heating temperatures or after different soaking durations up to 1 h. Quenching was performed by helium blowing (about −300 °C/s above 500 °C) to prevent ferrite formation during cooling.

Table 1 Chemical composition of the steel under investigation (wt%)

C	Mn	Si	P	S	Fe
0.15	1.48	0.013	0.01	27 ppm	bal

Microstructure characterization

All the microstructure analyses were performed at ¼ of the sheet thickness in the RD-ND plane (Rolling Direction—Direction Normal to the sheet surface). Two types of etchants were used for the metallographic investigations by optical microscopy (Olympus PMG 3): (i) Dino etching to reveal the ferrite + martensite microstructure (140 ml of distilled water, 100 ml of H_2O_2, 4 g of oxalic acid, 2 ml of H_2SO_4, and 1.5 ml of HF); (ii) Metabisulfite etching to quantify the austenite/martensite fraction (7 g of sodium metabisulfite in 100 ml of distilled water). This volume fraction was determined by optical image analysis and processing (gray-level thresholding method) using Aphelion software (copyright ADCIS S.A. and A.A.Imaging). An average value was measured on ten micrographs (120 × 90 μm^2). When reported, error-bars correspond to confidence interval at 95 %, i.e., $\approx \pm 2.\sigma^*/\sqrt{n}$, where σ* is the estimated standard error and n the number of micrographs.

Evaluation of recrystallized fraction

The fraction of recrystallized ferrite was determined using either Vickers hardness measurements (0.5 kg load) or Electron Back Scattered Diffraction (EBSD; Nordlys-F camera, Oxford Instruments) analysis on a JEOL 7001-F scanning electron microscope. The method using hardness measurements estimates the volume fraction of recrystallized ferrite (F^{ReX}) as the relative decrease of hardness between cold-rolled (H_v^{CR}), fully recrystallized, (H_v^{ReX}) and partially recrystallized (H_v^{PReX}) states, according to the following relation:

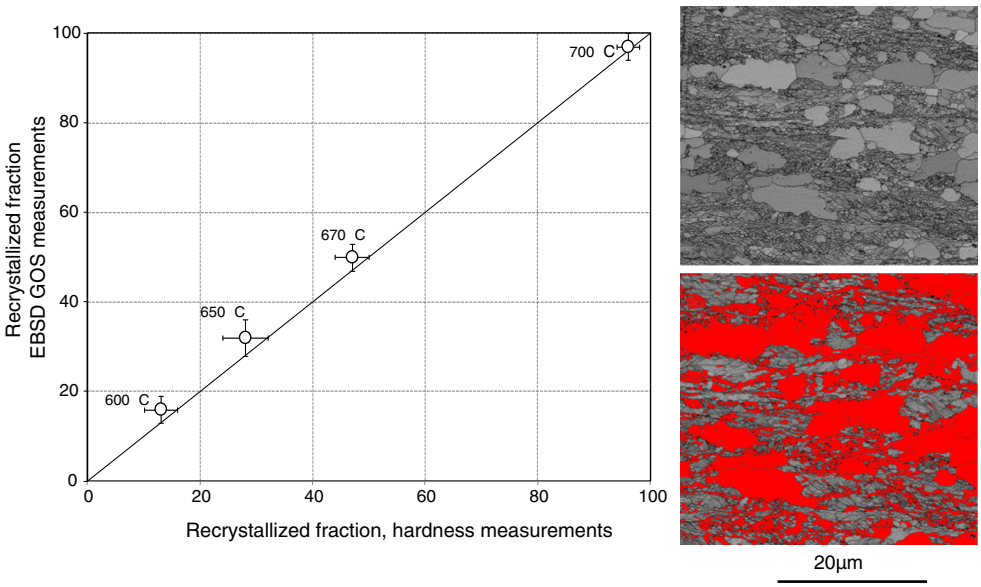

Fig. 1 Comparison of recrystallized ferrite fractions measured by Vickers hardness and EBSD–GOS for samples heated at 1 °C/s and quenched from 600, 650, 670, and 700 °C (no phase transformation). A magnification of an EBSD map is showed to highlight the GOS method (*upper map*: band contrast mapping; *lower map*: the recrystallized grains determined by the GOS method are highlighted in *red*) (Color figure online)

$$F^{\mathrm{ReX}} = \frac{H_{\mathrm{v}}^{\mathrm{cr}} - H_{\mathrm{v}}^{\mathrm{PReX}}}{H_{\mathrm{v}}^{\mathrm{cr}} - H_{\mathrm{v}}^{\mathrm{ReX}}}$$

Obviously, the hardness method only operates below Ac1 and is not applicable in the (ferrite + austenite) domain. Above Ac1, EBSD was used to estimate the recrystallized ferrite fraction. Samples for EBSD mapping were prepared following conventional metallographic sample preparation finished by mechanical polishing with a suspension of silica particles (OPS). The recrystallized ferrite fraction estimation was based on the Grain Orientation Spread (GOS) criterion [32]. Grains were identified using a misorientation angle threshold of 2°. Grains with a GOS lower than 1.5° were considered as recrystallized. To ensure a good correlation between both determined fractions, the recrystallized fractions during a slow heating (1 °C/s) before Ac1 were determined by both methods for samples quenched from 600, 650, 670, and 700 °C during heating. As for the metallographic analysis, error-bars correspond to confidence interval at 95 % obtained on three different EBSD maps. Figure 1 compares the results obtained by Vickers hardness and EBSD-GOS analysis. Both measured fractions are in very good agreement, with a correlation coefficient higher than 0.999. An extract of an EBSD map performed at 670 °C is showed to illustrate the GOS method. The upper map is represented in the band contrast mode when the lower one displays in red the recrystallized grains determined with the GOS method.

When the recrystallization and the phase transformation were occurring simultaneously, the following procedure was used to quantify the three constituents, i.e., martensite, deformed ferrite, and recrystallized ferrite. First, the martensite fraction was determined from optical micrographs as described in "Material" section. Then the ratio between deformed and recrystallized ferrite was determined using the EBSD–GOS method. For that purpose, martensite has to be previously eliminated from the EBSD map. This was done using a thresholding on the band slope value. This allowed the discrimination of about 80 % of the martensite. The rest was excluded manually by taking into account the grain size and the mean band contrast.

Results and discussion

Figure 2 presents the evolution of the volume fraction of deformed ferrite, recrystallized ferrite, and austenite as a function of the annealing temperature and time. Figure 4 reports various microstructures observed after quenching from different temperatures and times. The austenite (observed as martensite) appears in dark, the recrystallized grains in light gray, and the deformed grains in dark gray. Dino etching also reveals the grain boundaries. In the following, we will firstly discuss the global kinetics of recrystallization/transformation, then focus on the associated microstructure evolutions.

Kinetics of ferrite recrystallization and austenite formation

As can be seen on Figs. 2d and 4j–l, the recrystallization takes place in less than one min at 680 °C, which is under Ae1. The resulting distribution of grain sizes is rather heterogeneous, with an average size of about 2.3 µm. In pearlite-rich bands, the grains are much smaller than in the

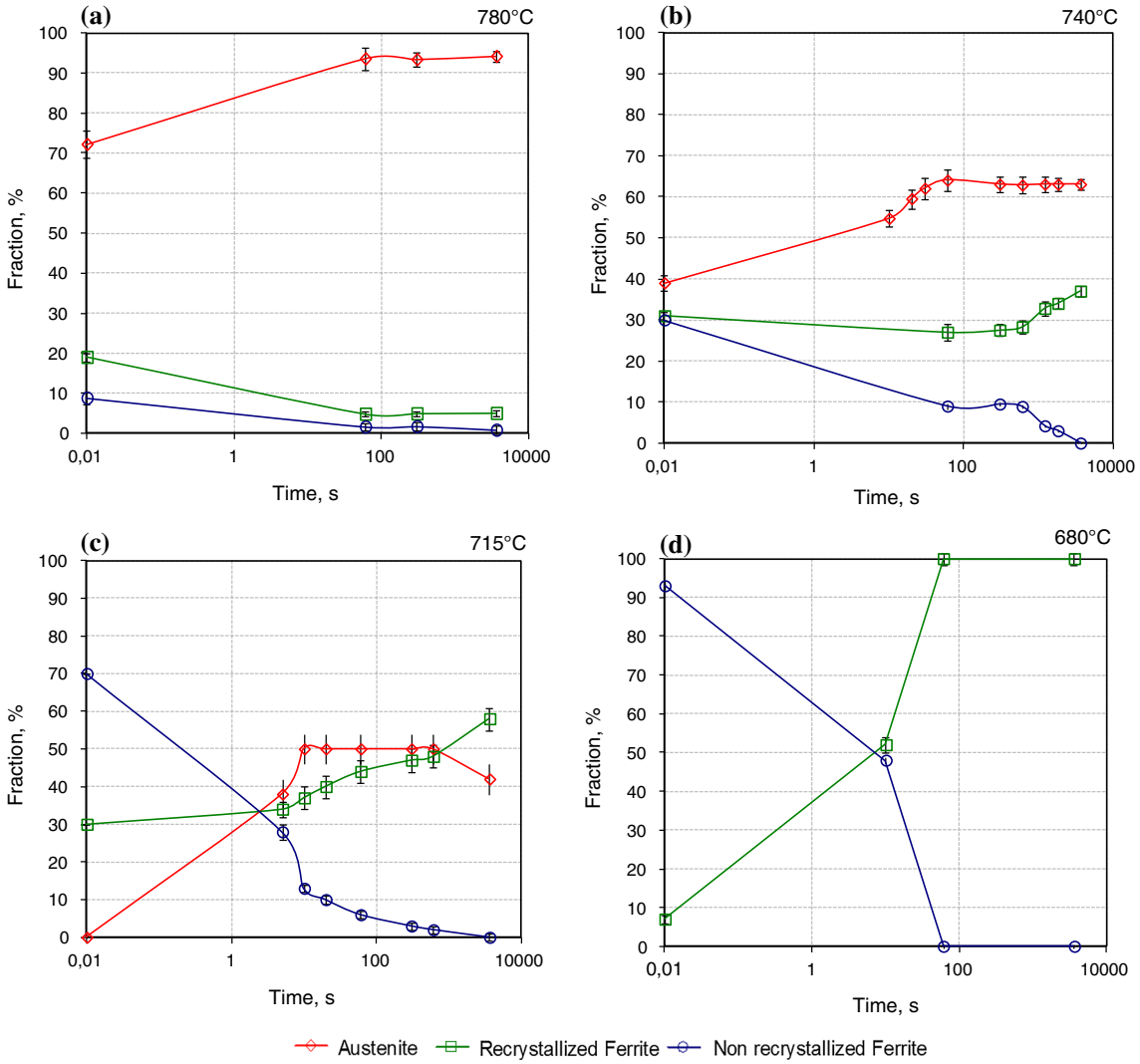

Fig. 2 Evolution of the different phase fractions during isothermal annealing at different temperatures after rapid heating (100 °C/s) (**a**) 780 °C (**b**) 740 °C (**c**) 715 °C (**d**) 680 °C

rest of the material. Although no deeper investigation of the recrystallization process was performed under Ae1, two reasons can be invoked to explain this observation: (i) deformation gradients are expected to be higher in pearlite regions, leading to a higher density of recrystallized nuclei; (ii) Growth of recrystallized grains may be hindered due to pinning by carbides.

Above Ae1, for all annealing temperatures, the austenite volume fraction reaches a plateau in less than one minute (Fig. 2a–c). In general, the maximum volume fraction of austenite is much higher than the austenite fraction under both OrthoEquilibrium (OE) and ParaEquilibrium (PE) calculated by ThermoCalc [33] (see Fig. 3). This unusual behavior is exacerbated at lower temperatures (below 740 °C) and was already reported in [9, 29] without any clear explanation. In order to explain the effect of high heating rate on kinetics of austenite formation, it was suggested in [30] that the heating rate would influence the nature of local equilibrium at the α/γ interface. This local equilibrium depending on the interaction between alloying elements such as manganese and the migrating interface, a transition between PE and OE conditions is expected to occur similarly to the ferrite transformation [34]. However, the results obtained below 740 °C do not support this explanation for the main reason that the measured volume fractions are much higher than both OE and PE ones. The results, especially those at 715 °C close to the eutectoid plateau, at which the driving force for austenite growth is classically low, would rather suggest a diffusionless transformation for austenite [35].

At 715 °C (Fig. 2c), when soaking begins, 30 % of the ferrite is already recrystallized but no austenite has already

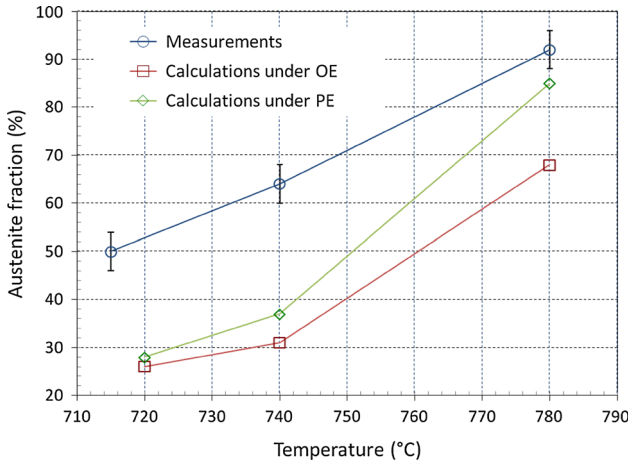

Fig. 3 Evolution of the maximum austenite fraction as a function of temperature. For comparison, the volume fraction of austenite under both orthoequilibrium and paraequilibrium is given

been formed. Then, austenite appears and rapidly reaches a plateau at about 45 % after 10 s. Meanwhile, the fraction of deformed ferrite strongly decreases while recrystallized one slightly but steadily increases. A different situation is observed at a higher temperature. At 740 °C (Fig. 2b), the initial recrystallized fraction is also 30 % but 40 % of austenite has already formed. Then, it continues to grow and reaches a plateau at about 60 % in less than one minute. Meanwhile, recrystallization of ferrite appears to be inhibited for more that 10 min before to slowly restart. The reasons for this inhibition are not clear. Different possible origins have been proposed in our previous article, which precisely focused on the mechanisms of the interaction between recrystallization and transformation at this temperature [30]. They are associated with a relaxation of the driving force for recrystallized nuclei after austenite formation took place. This was suggested by the observation that the last steps of recrystallization rather proceed by growth of already recrystallized grains and restoration of deformed ones (see also the discussion in "Resulting microstructures" section). At 780 °C (Fig. 2a), when annealing begins, the austenite fraction is already above 70 %, and it still increases up to 90 % in less than one min, at the expense of both recrystallized and deformed ferrites. Small amount of non-recrystallized ferrite persists after long soaking times, although fine evolutions can hardly be evidenced in that case with regard to the very small amounts of ferrite.

Obviously, the recrystallization kinetics is affected by the formation of austenite. At 680 °C, when no austenite is formed, the primary recrystallization is finished after one min only. At 715 °C, in the presence of austenite and despite a higher driving force, some deformed ferrite is still detected in the microstructure even after 5 min. The recrystallization rate decreases with the increasing austenite fraction. At moderate temperatures, an inhibition of the recrystallization is clearly evidenced. At high temperature, small amount of non-recrystallized ferrite persists after long soaking times.

Resulting microstructures

The interaction between recrystallization and austenite formation has a considerable influence on the microstructures at the end of the treatment. Representative optical microstructures are presented in Fig. 4 for different soaking times and temperatures. Figure 5 also shows band contrast EBSD maps showing the microstructure at higher magnification.

Relatively similar evolutions are observed at 715 and at 740 °C, characterized by heterogeneous recrystallization and development of anisotropic two-phase microstructures in the sense that the size of the grains depends on direction. The second phenomenon appears more marked at 740 °C. At 715 °C-0 min, no austenite is yet present. First, recrystallized grains appear scattered relatively homogeneously in the deformed microstructure. After 1 min, the amount of austenite has significantly increased, and some recrystallized grains appear elongated in the rolling direction. After 5 min, some very large grains are observed, resulting in a very heterogeneous but relatively more isotropic microstructure. At 740 °C-0 min, 40 % of austenite is already present, and the recrystallized ferrite already shows coarse anisotropic grains. This anisotropy persists and even increases during soaking. At the end of the treatment, very long and coarse ferrite grains are observed. At 780 °C-0 min, significant fractions of austenite and recrystallised ferrite are formed, with some sparse elongated ferrite grains. However, due to the percolation of austenite growing at the expense of both types of ferrite, anisotropy progressively disappears and the microstructure appears relatively homogeneous and equiaxed at the end of the treatment.

EBSD characterization allows the discrimination of deformed and recrystallized ferrite whatever the grain size (Fig. 5). Deeper analysis of EBSD maps showed that the final shape of the recrystallized ferrite grains is constrained by the spatial distribution of austenite. As austenite nucleates around globular cementite, it is preferentially formed in carbides-rich (Mn-rich) bands. The presence of Mn-rich bands have been highlighted and investigated in a previous study on the same material [30]. This tendency is also promoted by the fact that Mn is a gamma-stabilizer element. On the contrary, the rate of growth of recrystallized grains is reduced by Mn [36], leading to hindering of the recrystallization. After nucleation, further growth of austenite is very rapid. The deformed ferrite grains, which

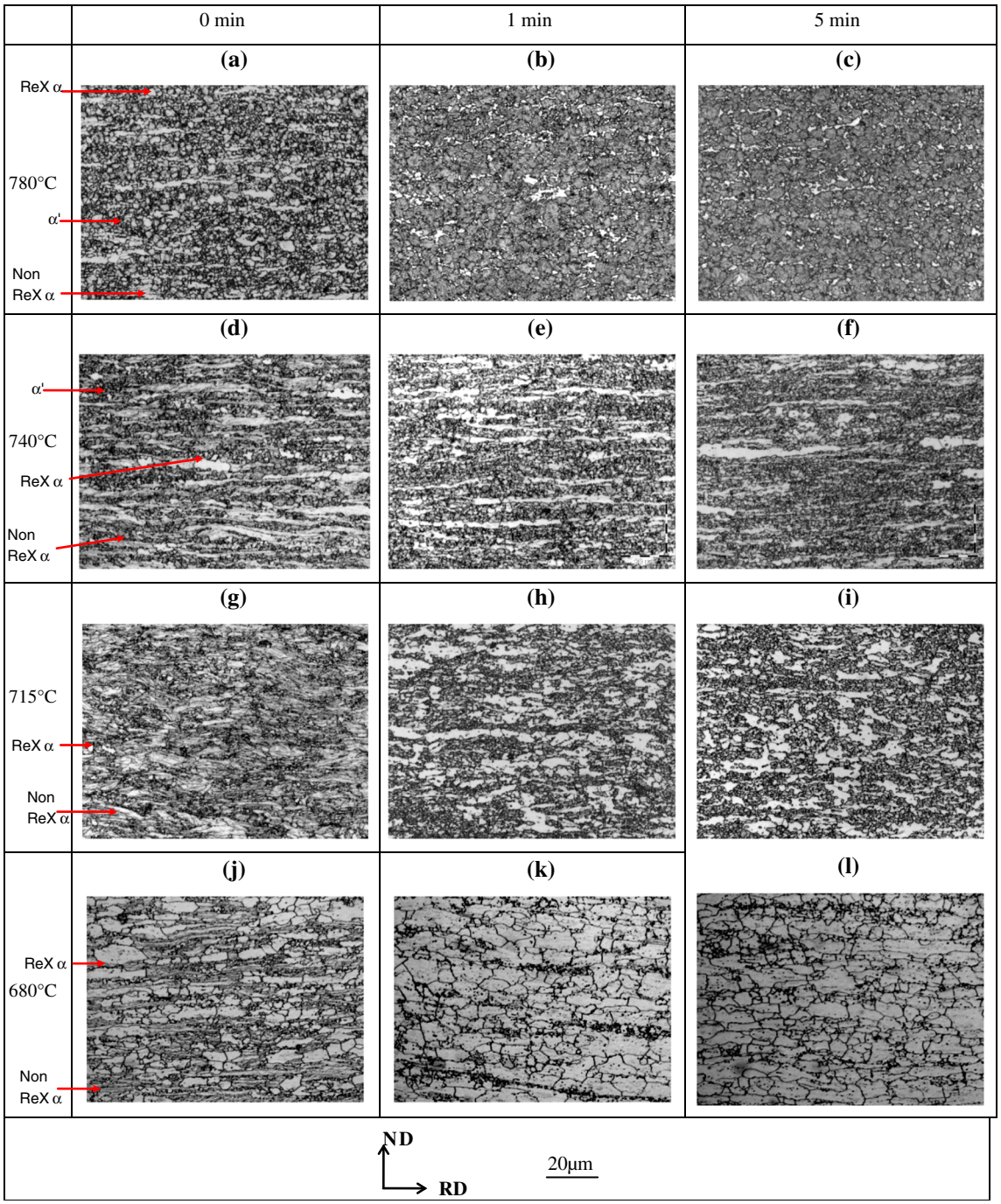

Fig. 4 optical micrographs obtained on microstructures after annealing at 780, 740, 715, and 680 °C for 0, 1, and 5 min after rapid heating (100 °C/s)

were still present when austenite transformation took place, are afterward only able to recrystallize from the already present ferrite nuclei, due to the inhibition of additive nucleation. They developed constrained by the topology of austenite, i.e., parallel to the direction of segregated bands. In other words, austenite grains act as pinning obstacles for the moving boundaries between deformed and recrystallized ferrite. Consequently, microstructure anisotropy is clearly related to the influence of Mn segregation on austenite transformation. A maximum effect seems to be obtained in a temperature range where the ferrite recrystallization is constrained by 40–60 % of austenite.

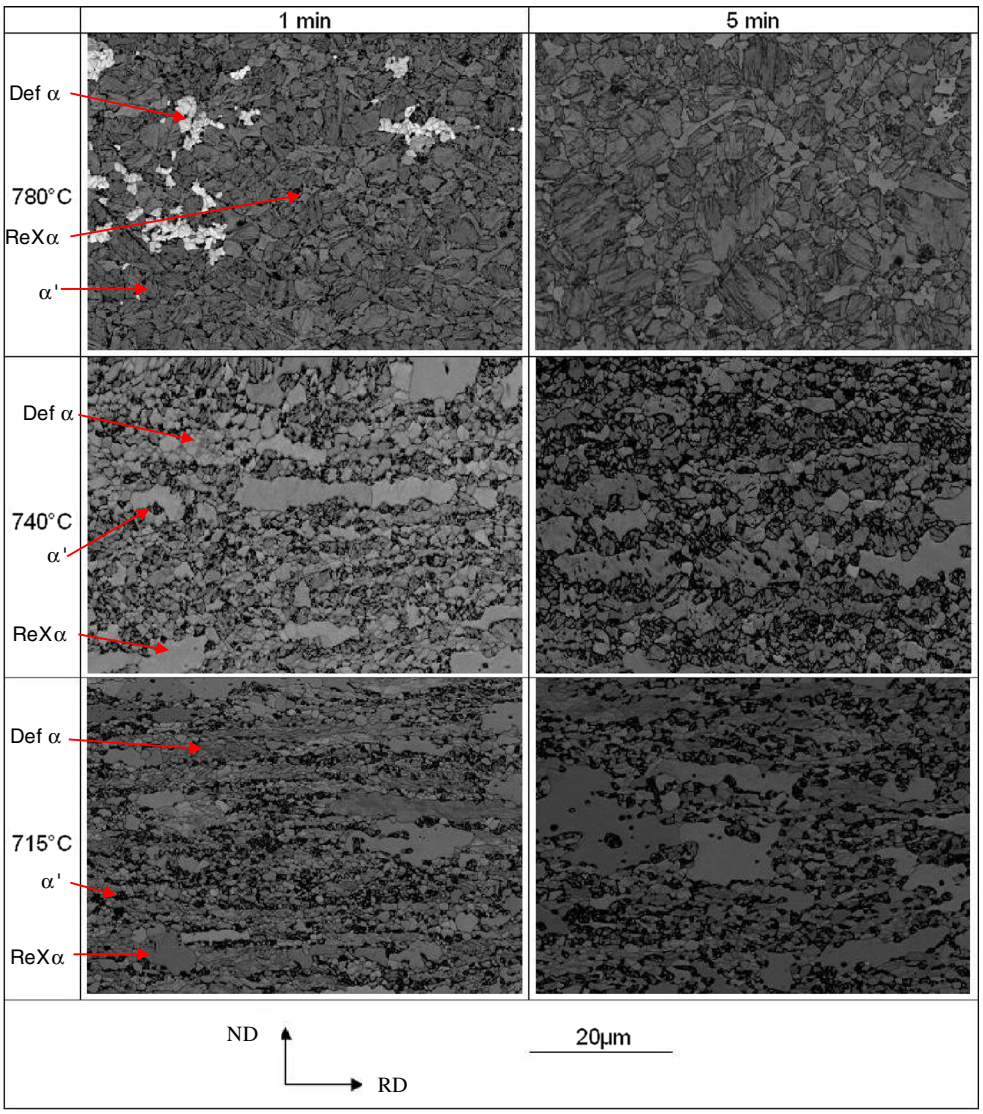

Fig. 5 EBSD band contrast maps obtained on microstructures after annealing at 715, 740, and 780 °C for 1 and 5 min after rapid heating (100 °C/s). The different constituents are indicated: recrystallized ferrite (ReX α), deformed ferrite (Def α), and martensite (α′). In the microstructure at 780 °C - 1′, deformed ferrite is highlighted in *light gray*

Conclusions

The present work studied the interaction between the ferrite recrystallization and the austenite formation in dual-phase steels. This interaction was forced by a high heating rate (100 °C/s) from room temperature (75 % cold-rolled microstructure) up to different temperatures below and within the intercritical domain (680, 715, 740, 780 °C). The global kinetics of evolution of the three main constituents of the microstructure—deformed ferrite, recrystallized ferrite, and austenite—were quantified at these four temperatures. The development of grain size heterogeneity and microstructure anisotropy was followed by microscopic observations coupled with EBSD analyses. The main conclusions are as follows:

- The austenite formation was found to proceed very rapidly (in less than 1 min) for all the temperatures tested in the intercritical domain; the measured final volume fractions (stable over a time range of 1 h) were higher than the expected equilibrium values.
- The nucleation of austenite is heterogeneous; it preferentially takes place in the Mn-rich bands due to the presence of cementite particles and to the fact that Mn is a gamma-former element.
- The formation of austenite has a strong delaying effect on the subsequent growth of recrystallized ferrite; this effect was attributed to the inhibition of recrystallized seeds nucleation in presence of austenite. The ferrite recrystallization finishes by grain growth and restoration.

– Strong microstructure heterogeneity and anisotropy can result from the competitive growth of austenite and recrystallized ferrite; the maximum of anisotropy is observed for temperatures where the final recrystallization/restoration step is constrained by the presence of about 40–60 % of austenite; at lower temperatures, the pinning effect of austenite is lower but growth of some ferrite grain can be observed; at higher temperatures, high amount of austenite results in finer and more homogeneous microstructures.

References

1. Llewellyn DT, Hillis DJ (1996) Dual phase steels. Ironmak Steelmak 23:471–478
2. Militzer M (2006) Microstructure evolution in dual-phase steels. Trans Indian Inst Met 59:711–724
3. Kuziak R, Kawalla R, Waengler S (2008) Advanced high strength steels for automotive industry: a review. Arch Civ Mech Eng 8:103–117
4. Bouaziz O, Zurob H, Huang M (2013) Driving force and logic of development of advanced high strength steels for automotive applications. Steel Res Int 84:937–947
5. Speich G, Demarest V, Miller R (1981) Formation of austenite during intercritical annealing of dual-phase steels. Met Trans A 12:1419
6. Garcia CI, Deardo AJ (1981) Formation of austenite in 1.5 pct Mn steels. Met Trans A 12:521
7. Tokizane M, Matsumura N, Tsuzaki K, Maki T, Tamura I (1982) Recrystallization and formation of austenite in deformed lath martensitic structure of low carbon steels. Met Trans A 13:1379
8. Yang D, Brown E, Matlock D, Krauss G (1985) The Formation of austenite at low intercritical annealing temperatures. Met Trans A 16:1523
9. Huang J, Poole WJ, Militzer M (2004) Austenite formation during intercritical annealing. Metall Mater Trans A 35A:3363
10. Leslie W, Plecity F, Michalak J (1961) Recrystallization of iron and iron-manganese alloys. Trans Metall Soc AIME 221:691–700
11. Petrov R, Kestens L, Houbaert Y (2001) Recrystallization of a cold rolled trip-assisted steel during reheating for intercritical annealling. ISIJ Int 41:883
12. Maruyama N, Ogawa T, Takahashi M (2007) Recrystallization at intercritical annealing in low carbon steels. In: Kang SJL, Huh MY, Hwang NM, Homma H, Ushioda K, Ikuhara Y (eds) Recrystallization and Grain Growth III, Pts 1 and 2, 558-559 edn. Trans Tech Publications Ltd, Stafa-Zurich
13. Dillien S, Seefeld M, Allain S, Bouaziz O, Van Houtte P (2010) EBSD study of the substructure development with cold deformation of dual phase steel. Mater Sci Eng A 527:947–953
14. Tian Y, Kraft R (1987) Mechanisms of pearlite spheroidization. Met Trans A 18:1403–1414
15. Yang DZ, Brown EL, Matlock DK, Krauss G (1985) Ferrite recrystallization and austenite formation in cold rolled intercritically annealed steel. Metall Trans A 16A:1385–1392
16. Ågren J, Abe H, Suzuki T, Sakuma Y (1986) The dissolution of cementite in a low-carbon steel during isothermal annealing at 700-Degrees-C. Met Trans A 17:617
17. Goune M, Maugis P, Drillet J (2012) A criterion for the change from fast to slow regime of cementite dissolution in Fe–C–Mn steels. J Mater Sci Technol 28:728–736
18. Atkinson C, Akbay T, Reed RC (1995) Theory for reaustenitisation from ferrite/cementite mixtures in Fe–C–X steels. Acta Metall Mater 43:2013–2031
19. Caballero FG, Capdevila C, de Garcia Andrés C (2001) Modelling of kinetics of austenite formation in steels with different initial microstructures. ISIJ Int 41(10):1093–1102
20. Toji Y, Yamashita T, Nakajima K, Okuda K, Matsuda H, Hasegawa K, Seto K (2011) Effect of Mn partitioning during intercritical annealing. ISIJ Int 51(5):818–825
21. Mohanty RR, Girina OA, Fonstein NM (2011) Effect of heating rate on the austenite formation in low-carbon high-strength steels annealed in the intercritical region. Metall Mater Trans A 42A:3680–3690
22. Azizi-Alizamini H, Militzer M, Poole WJ (2011) Formation of ultrafine grained dual phase steels through rapid heating. ISIJ Int 51:958–964
23. Bleck W, Phiu-On K (2005) Microalloying of cold-formable multi phase steel grades. In: Rodriguez-Ibabe JM, Gutierrez I, Lopez B, Iza-Mendia I (eds) Microalloying for new steel processes and applications. Trans Tech Publications Ltd, Stafa-Zurich, pp 97–112
24. Hayami S, Furukawa T, Gondoh H, Takechi H (1979) Recent developments in formable hot and cold rolled HSLA including dual-phase sheet steels. In: Davenport AT (ed) Formable HSLA and dual-phase steels. TMS, New York, pp 167–180
25. Andrade-Carozzo V, Jacques PJ (2007) Interactions between recrystallization and phase transformations during annealing of cold rolled Nb-added TRIP-aided steels. Mater Sci Forum 539–543:4649–4654
26. Ogawa T, Maruyama N, Sugiura N, Yoshinaga N (2010) Incomplete recrystallization and subsequent microstructural evolution during intercritical annealing in cold-rolled low carbon steels. ISIJ Int 50:469–475
27. Peranio N, Li YJ, Roters F, Raabe D (2010) Microstructure and texture evolution in dualphase steels: competition between recovery, recrystallization, and phase transformation. Mater Sci Eng A 527:4161–4168
28. Zheng C, Raabe D (2013) Interaction between recrystallization and phase transformation during intercritical annealing in a cold-rolled dual-phase steel: a cellular automaton model. Acta Mater 61:5504–5517
29. Kulakov M, Poole WJ, Militzer M (2013) The effect of the initial microstructure on recrystallization and austenite formation in a DP600 steel. Metall Mater Trans A 44:3564–3576
30. Chbihi A, Barbier D, Germain L, Hazotte A, Gouné M (2014) Interactions between ferrite recrystallization and austenite formation in high strength steels. J Mater Sci 49:3608–3621. doi:10.1007/s10853-014-8029-2
31. Karmakar A, Ghosh M, Chakrabarti D (2013) Cold rolling and intercritical annealing of low carbon steel: effect of initial microstructure and heating rate. Mater Sci Eng A 564:389–399
32. Dziaszyk S, Payton EJ, Friedel F, Marx V, Eggeler G (2010) On the characterization of recrystallized fraction using electron backscatter diffraction: a direct comparison to local hardness in an IF steel using nanoindentation. Mater Sci Eng A 527:7854–7864
33. Thermocalc software, P16 version, Stockholm, Sweden
34. Purdy G, Ågren J, Borgenstam A et al (2011) ALEMI: a Ten-Year history of discussions of alloying-element interactions with migrating interfaces. Metall Mater Trans A 42:3703–3718
35. Han J, Lee Y-K (2014) Acta Mater 67:354
36. Leslie WC, Plecity FJ, Michalak JT (1961) Recrystallization of iron and iron-manganese alloys. Trans Metall Soc AIME 221:691–700